ACTIVATED CARBON FROM ANTHRACITE[1]

Masayuki Kawahata[2] and P. L. Walker, Jr.[3]

The Pennsylvania State University
University Park, Pennsylvania

The paper is the first report of a systematic study on the manufacturing process of activated carbons from anthracite, using a large bench scale fluidization reactor. A St. Nicholas anthracite was activated with CO_2, following a preliminary study of fluidization of anthracite particles to determine the fluidization conditions best suited for this experiment. A particle size, 42x65 Tyler mesh, and flow rate of CO_2, 0.037 ft.^{3}/min., were chosen from the preliminary study. The reaction temperature was varied from 800 to 950°C and the degree of burn-off ranged from 8 to 65%.*

The activation energy found for the reaction of CO_2 with the anthracite was about 50 kcal./mole. The reaction-rate-controlling step at the temperatures employed was a combination of the rate of diffusion of CO_2 into the internal pore structure of the anthracite and the intrinsic chemical rate.

Properties necessary to characterize the pore structure of the activated anthracites, including surface area, pore volume, and pore volume distribution were investigated. The surface area increased linearly with burn-off from 1.5 m.^{2}/g.* in raw anthracite to 1890 m.^{2}/g.* in anthracite activated to 65% burn-off at 850°C.

The adsorptive capacity of the activated anthracites for CCl_4 also increased linearly with burn-off. The effect of activation temperature on the adsorptive capacity was not significant over the temperature range between 800 and 900°C. The optimum percentage of burn-off was determined to be 53.4%. At this burn-off, the adsorptive capacity was 0.70 g.CCl_4/g.*

The pore structure data of two representative activated anthracites, together with their CCl_4-adsorption characteristics, were compared to those of two commercial bituminous coal-based activated carbons.

INTRODUCTION

Activated carbons for vapor adsorption processes are used in the chemical industry for solvent recovery, gas separation, odor removal, and fractional adsorption. These activated carbons are manufactured by mild oxidation of char produced from various carbonaceous materials such as lignite, bituminous coal, wood, and nutshells. The history and nature of the carbonaceous material, as well as process conditions, determine the properties of the activated carbon produced. It is generally agreed that activated carbons owe their high adsorptive capacities to an internal structure which consists of a large number of interconnecting, fine pores. This internal porosity has been described by parameters such as pore volume, pore surface area, and pore size distribution in order to better understand the adsorptive characteristics of activated carbons.

Anthracite has a considerable porosity, with a large fraction of the porosity in pore sizes of molecular dimensions (1, 2, 3). Suitably treated, this fine pore structure of anthracite could be utilized for the successful production of activated carbons. Clendenin, Griffiths, and Wright (4) studied a steam activation process for various Pennsylvania anthracites of different volatile matter contents using a fixed bed reactor. The

[1] Based, in part, on a Ph.D. thesis submitted by M. Kawahata to the Graduate School of The Pennsylvania State University, January, 1960.

[2] Research Associate in Fuel Technology.

[3] Chairman of the Mineral Technology Division and Professor of Fuel Technology.

* Percentage burn-offs, physical property data, and adsorption capacities for CCl_4 for all samples are given on a mineral matter free basis (m.m.f.b.).

process conditions studied were activation temperature, amount of burn-off, steam flow rate, and anthracite particle size. The carbons produced were examined by various standard tests used to characterize commercial activated carbons. It was concluded that anthracite could be a suitable raw material for the production of activated carbons. Hassler (5, 6) studied a process for producing activated carbon from anthracite in a fluidized bed. At a weight loss of 20%, the anthracite activated with steam had a surface area of about 800 $m.^2/g$. The production of activated carbon for liquid phase adsorption was Hassler's primary purpose and inevitably the process was rather complex, being accompanied by the impregnation of the activated carbon with inorganic chemicals, followed by roasting and secondary steam activation. In both of the above studies the pore structure of the product carbons was not clearly or completely delineated. Numerous papers have been published on the pore structure of activated carbons and on their adsorption characteristics for various adsorbates. However, the manufacturing process conditions used for activation of these carbons have not been made available in the literature.

It was felt, therefore, that in this research a systematic study of the effect of process conditions on the pore structure and adsorption characteristics of activated anthracites should be made. In this way, commercial possibilities for anthracite as a source of activated carbon could be thoroughly explored. The purpose of this research then was concerned with the following objectives: (1) to investigate the effect of the process conditions on the pore structure of the activated anthracites and to clarify the mechanism of development of pore structure in anthracite as activation proceeds, (2) to investigate the adsorptive characteristics of activated anthracites for organic vapors as a function of the process conditions and their pore structures, and (3) to evaluate activated anthracites, by comparing their properties with activated carbons marketed commercially.

This paper covers the initial phase of a systematic study, with the work being restricted to activation of one anthracite of fixed particle size, using CO_2 as the oxidizing gas. The paper presents the results pertinent to objectives (2) and (3) listed above. The major results pertinent to objective (1) will be published elsewhere.

EXPERIMENTAL

PRELIMINARY STUDY ON FLUIDIZATION OF ANTHRACITE

For the experimental activation reactor, fluidized bed techniques were employed. In general, a good gas-solid contact and a uniform temperature distribution in the reactor are desirable characteristics realized by using fluidization techniques. However, the most important reason for employing fluidization techniques in this investigation was based on the desire to acquire a uniform degree of activation of anthracite particles through the entire reactor bed. If particle size and gas flow rate are suitably chosen, the fluidized bed shows an aggregative fluidization state. In this state, a good bottom-to-top solid turn-over may be obtained, resulting in the desired uniformity of activation for the entire sample.

Numerous papers have been published on fluidization techniques but, because of the complexity of the problem, no generalized formulation of the fluidization conditions was quantitatively satisfactory. Consequently, the most positive way to achieve the purpose of this study seemed to be to use direct observation of the behavior of fluidization of anthracite particles in a specified system. Therefore, prior to commencing with the activation experiments, a fluidization column, consisting of a glass tube having a diameter similar to that of the activation reactor, was built, and the fluidization behavior of anthracite particles was observed. The inside diameter of the glass tube was 1.95 in. The anthracite sample was placed on a porous alundum disc, which was fastened to the glass tube with a gland. Air was introduced from the bottom as the fluidization medium. Starting from fixed bed conditions, the flow rate of air was increased gradually. With increasing gas flow rate, the fluidization state progressively changed from a quiescent, to an aggregative, to a slugging condition. The quiescent condition was characterized by a local turbulence but not an over-all solid turn-over. The aggregative condition was characterized by appreciable solids turn-over. The slugging condition was characterized by growing of bubbles to a size equal to the diameter of the tube before escaping the bed and thus creating gas pockets pushing plugs of particles up the tube. At each increment of gas-flow-rate increase, the

pressure drop across the bed, the height of the bed, and the condition of fluidization were recorded. From these observations, the following determinations were made: (1) particle densities of various particle cuts of anthracite, (2) flow velocity of gas and bed density at each minimum fluidization condition, and (3) ranges of gas flow rates where the fluidization condition showed quiescent, aggregative, and slugging states.

An anthracite from the Glen Alden Corp. was used for this preliminary work. The particle cuts chosen were 25x40, 40x60, 60x80, and 80x140 mesh (U. S. standard sieve series). The method used to determine particle density was described by Williams (7). The values of particle density, γ_a, and minimum fluidization bed density, γ_{bc}, determined experimentally are listed in Table I. Using these values and employing the method proposed by Leva, et al. (8, 9), minimum fluidization velocities, u_{mf}, where the quiescent condition should commence, were calculated (predicted) as a function of particle size and are listed in Table I. The critical flow rate of gas (observed

TABLE I

Particle Density, Critical Bulk Density and Calculated Minimum Fluidization Velocity for Various Particle Sizes of a Glen Alden Anthracite

Particle size U. S. sieve	Particle diameter inch	γ_a lb./ft.^{3}	γ_{bc} lb./ft.^{3}	u_{mf} ft./sec.
25 x 40	0.0218	81.5	45.5	0.64
40 x 60	0.0127	83.5	43.9	0.22
60 x 80	0.0083	84.7	40.5	0.11
80 x 140	0.0053	89.6	39.4	0.051

experimentally), at which quiescent, aggregative, and slugging conditions commenced are listed in Table II. The agreement between the predicted and observed minimum fluidization velocities was quite satisfactory.

In order to correlate the three critical flow rates against particle size and particle density, ln $(D_p^3\gamma_a)$† was plotted against ln $(D_pG\mu/\gamma_f)$ in

† Refer to the end of the paper for a definition of symbols for preliminary study on fluidization.

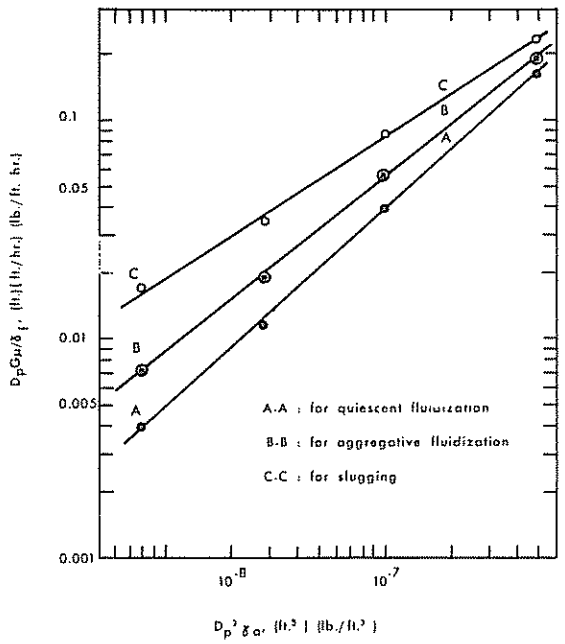

CRITICAL FLOW RATES FOR QUIESCENT, AGGREGATIVE AND SLUGGING CONDITIONS IN THE FLUIDIZED BED OF ANTHRACITE (FLUID : AIR)

Figure 1

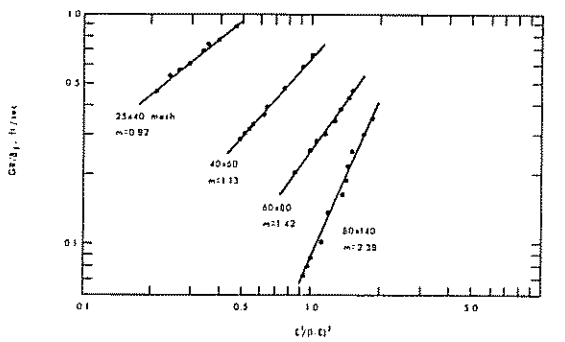

PLOT OF GR/α_f AGAINST $c^2/(\beta\cdot c)^2$ TO OBTAIN m FOR ANTHRACITE IN THE FLUIDIZED BED (FLUID : AIR)

Figure 2

Figure 1. This plot was used to determine the appropriate gas flow rates for fluidization in later activation experiments. It was understood that the group, $D_p^3\gamma_a$, varied with burn-off in the activation process because of a continuously decreasing γ_a. However, the group could be calculated for various degrees of burn-off, provided the initial value of γ_a was known. Thus, using Figure 1, it was possible to determine an appropriate gas flow rate for the entire activation run, such that aggregative fluidization conditions could be obtained for various degrees of

TABLE II

Critical Flow Rates under Quiescent, Aggregative, and Slugging Conditions for Various Particle Sizes of a Glen Alden Anthracite

		Quiescent fluidization		Aggregative fluidization		Slugging conditions	
Particle diameter inch	$(D_p^3\gamma_g)\times10^8$	u_{mf}	$(D_pG\mu/\gamma_f)\times10^2$	u_{ma}	$(D_pG\mu/\gamma_f)\times10^2$	u_{ms}	$(D_pG\mu/\gamma_f)\times10^2$
0.0218	48.7	0.60	16.2	0.70	19.2	0.85	23.6
0.0127	9.90	0.24	3.96	0.35	5.70	0.53	8.63
0.0083	2.81	0.11	1.23	0.18	1.92	0.33	3.45
0.0053	0.77	0.06	0.41	0.11	0.74	0.25	1.73

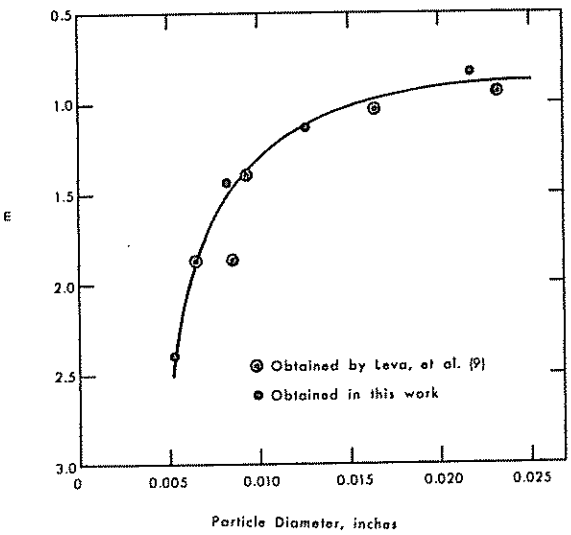

VALUES OF m FOR ANTHRACITE PARTICLES OF VARIOUS SIZES IN A FLUIDIZED BED (FLUID : AIR)

Figure 3

activation and reaction temperatures. In Figure 1, three straight lines were obtained: AA, BB, and CC corresponding to the critical flow rates for quiescent, aggregative, and slugging conditions, respectively. It is seen that the range of gas flow rate which produced the aggregative fluidization condition narrowed as the particle size was increased. Aggregative fluidization was obtained at a flow rate ranging from 1.3 u_{mf} to 1.6 u_{mf} for 25x40 mesh particles and from 1.8 u_{mf} to 4.3 u_{mf} for 80x140 mesh particles.

In Figure 2, ln (GR/γ_f) was plotted against ln $[(\epsilon^3/(1-\epsilon)^2]$ for various particle sizes. According to Leva, et al. (8, 9), the slope of this plot indicates the degree of gas-solid contact. A slope, m, of 1.0 is regarded as ideal, while deviations from 1.0 indicate less ideal gas-solid contact. The value of m determined was plotted against particle size in Figure 3. The values of m for anthracite obtained by Leva, et al. (8, 9) are also shown in Figure 3. The application of these fluidization correlations to the activation experiments will be described in a later section.

ACTIVATION APPARATUS

A flow sheet of the apparatus is shown in Figure 4. The preheater and reactor were made of Hastelloy-C heat-resistant alloy and both were heated externally by Kanthal electric resistance ribbon. The preheater dimensions were 1.61 in. inside diameter, 0.14 in. wall thickness, and 2.5 ft. long. Inside the preheater tube, copper turnings were packed to improve heat transfer from the wall. The Kanthal ribbon was wound over alundum tubes of $\frac{1}{4}$ in. thickness, which were assembled from cylindrical half sections. An $\frac{1}{8}$ in. layer of alundum cement covered the ribbon to keep it in place. The whole preheater tube was insulated with a 3 in. layer of Thermoflex high temperature insulation felt (Johns Manville Co.) and with a 5 in. thick magnesia pipe. The maximum power input to the preheater was 4 kilowatts. A chromel-alumel thermocouple, connected to a temperature controller, was embedded

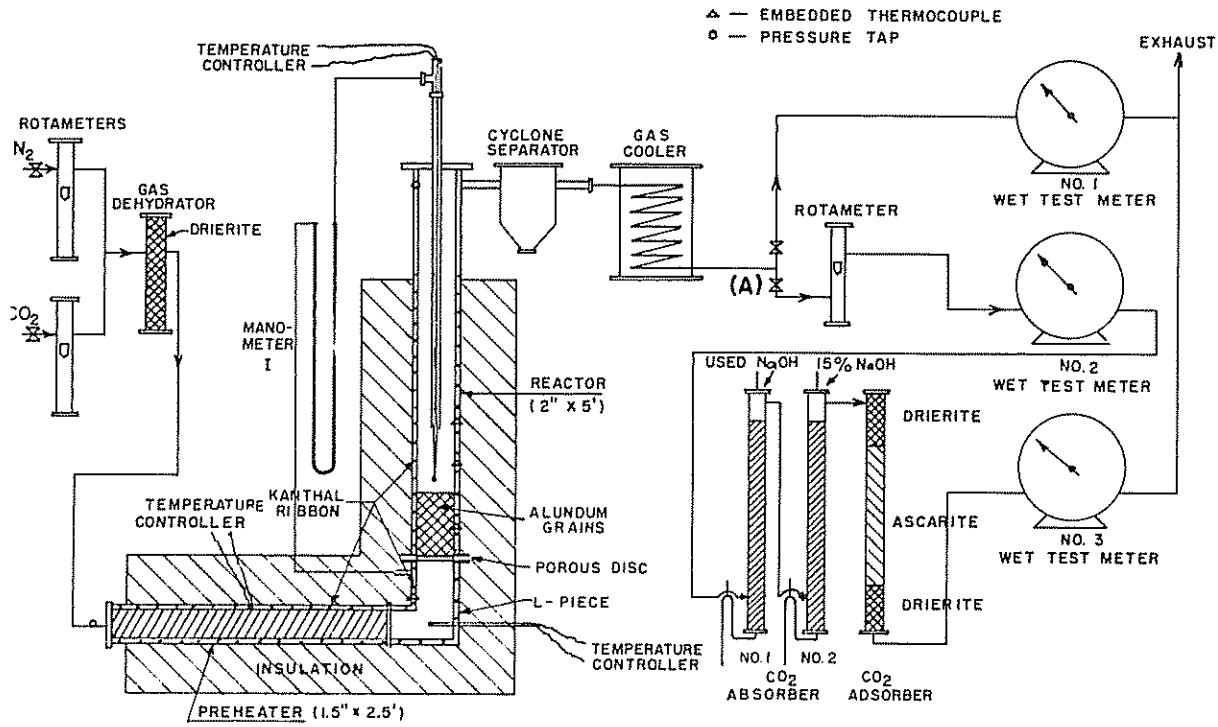

FIGURE 4 – APPARATUS FOR ACTIVATION OF ANTHRACITE

in the wall at the middle of the preheater section.

The reactor dimensions were 1.94 in. inside diameter, 0.20 in. wall thickness, and 5 ft. long. The L-piece and bottom 4 feet of the reactor were heated and insulated in the same manner as was the preheater. The maximum power input to the reactor was 4 kilowatts. To support the charged sample in the reactor, there was inserted between the flanges of the reactor and L-piece a porous alundum disc, 2.5 in. inside diameter and $\frac{1}{4}$ in. in thickness contained in a stainless steel ring. In addition, a 10 to 12 in. depth of 10x15 mesh (Tyler) alundum grains was maintained on the porous disc in order to achieve a uniform distribution of the fluidization gases.

A Hastelloy–C $\frac{1}{4}$ in. tube running vertically down the center of the reactor was used as a pressure probe. By using this pressure probe in conjunction with the pressure tap just below the porous disc, the pressure drop across the fluidized bed of anthracite could be determined. The vertical pressure probe also served two additional purposes: (1) as a guide tube for a chromel-alumel thermocouple (insulated with twin bore porcelain tubing) used to measure the reaction temperature, and (2) as a passage for samples when they were fed into or removed from the reactor. The pressure probe, fastened by a gland, had a pointer which lined up against a scale. From the location of the pointer, the position of the thermocouple in the reactor was known. By moving the probe vertically, it was possible to measure a vertical temperature profile in the reactor. The thermocouple was connected to a temperature controller to regulate the reaction temperature. Other points where thermocouples were installed are shown in Figure 4.

Carbon dioxide and N_2 were taken from cylinders. The purity of the gases were 99.99 and 99.95%, respectively. Traces of impurities were removed by passing the gases through Drierite columns and then through copper turnings in the preheater. The flow rate of gases was metered by rotameters. A cyclone separator and a gas cooler were attached to the system. Two wet test meters, two absorption columns, and an adsorption column were used to analyze the product gas during the activation process. A NaOH solution, fed dropwise from the top of the absorbers and a 50-50 mixture of Ascarite and

porcelain grains in the subsequent adsorber eliminated CO_2 from the product gases. Since only the reaction $C + CO_2 \rightarrow 2CO$ was operative during the activation run, it was possible to calculate the amount of carbon gasified as a function of time from measurements of the effluent gas volume and the concentration of CO in the effluent gas at selected time intervals.

APPARATUS FOR STUDIES ON PORE STRUCTURES

The activated anthracites were characterized by the following physical data: surface areas, He and apparent densities, total open pore volume, and pore volume distributions. A volumetric low-temperature N_2 adsorption apparatus, a mercury porosimeter, and a He density apparatus, used for these studies, are described in detail elsewhere (10, 11, 12).

APPARATUS FOR STUDIES ON ADSORPTIVE CHARACTERISTICS OF ORGANIC VAPORS

A flow diagram of the apparatus is shown in Figure 5. The apparatus was essentially a regular adsorption system utilizing a flow method. A thermal conductivity cell gas analyzer (Beckman Co.) and a potentiometric recorder (Brown Electronik) were used to detect the concentration of organic vapors in the effluent gas. Nitrogen, supplied from a cylinder, passed through the reference side of the thermal conductivity cell analyzer and then split into two streams. Both lines had a capillary flow meter, with the indicated flow rate being adjusted to the desired value by a needle valve. Nitrogen in line *A* was saturated with an organic vapor while passing through two vaporizers. An ice bath or a constant temperature bath was used to maintain a constant concentration of the organic vapor in the N_2 stream. The N_2 containing the organic vapor was diluted by adding N_2 from line *B*, and the resultant mixture was fed into the adsorber (maintained at 25°C.), where the adsorbent to be tested was placed. The effluent gas from the adsorber passed through the measuring side of the thermal conductivity cell analyzer and was then led to a wet test meter.

EXPERIMENTAL ACTIVATION CONDITIONS AND PROCEDURES

Samples—An anthracite from the St. Nicholas breaker of the Reading Anthracite Company

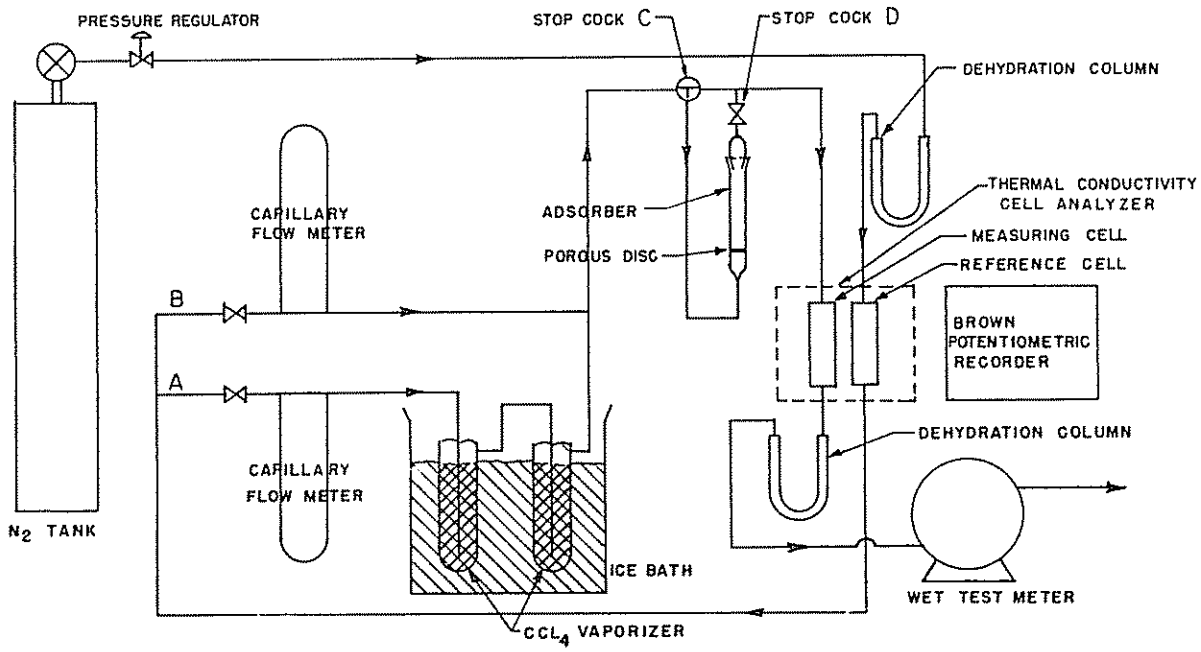

FIGURE 5 - APPARATUS FOR DYNAMIC ADSORPTION

was used for all the activation runs reported. The anthracite had a surface area of 1.5 m.²/g., as determined by N_2 adsorption at 78°K. The proximate analysis of this anthracite is shown in Table III.

TABLE III
Proximate Analysis of St. Nicholas Anthracite
(as received)

Moisture	1.1%
Volatile Matter	3.0
Ash	7.7
Fixed Carbon	88.2

Two bituminous coal-based activated carbons (designated by us as PC1 and PC2), supplied by the Pittsburgh Chemical Company, were compared both as to properties and adsorptive capacity for CCl_4 with the activated anthracites.

Activation temperature and degree of burn-off—Using two process variables, that is, reaction temperature and degree of burn-off, the first series of experiments was designed to set a two-way classification with four levels of each variable. In this experimental series, the maximum degree of burn-off studied was 38% over the temperature range 800 to 950°C. From the experimental results of this series, a second series of experiments was conducted in which the degree of burn-off was extended to 65% but the range of activation temperatures limited to 850 to 950°C. The maximum temperature gradient in the vertical direction of the fluidized bed was 0.5°C. per cm. of bed height. At the 95% confidence limit, the burn-off found experimentally following the activation run (by weighing the product) agreed to within ±1% with the desired burn-off.

Weight of samples used in activator—The experimental runs were stopped at the desired percentages of burn-off. A part of the activated sample was set aside for a study of its physical and adsorptive properties and the remainder of the sample was used for successive runs at higher percentages of burn-off. Therefore, the initial weight of the sample was varied depending on the percentage of burn-off which it underwent. In the first and second series of experiments, the starting weight of devolatilized anthracite was 225 and 200 g., respectively.

Particle size and rate of gas flow—On the basis of the data obtained from the preliminary fluidization studies, a particle size of 42x65 mesh (Tyler) was chosen for activation. This particle cut corresponds to an average diameter of 0.0116 in. For this particle size, $m = 1.2$, as shown in Figure 3. An actual test on this particle size of St. Nicholas anthracite using CO_2 as the fluidizing gas gave $m = 1.0$. The particle density of the 42x65 mesh fraction of devolatilized anthracite was determined to be 91.7 lb./ft.³ [using the Williams' method (6)], resulting in a value of 8.26×10^{-8} lb. for $D_p^3\gamma_a$. Taking into account the variation of $D_p\gamma_a$ with burn-off and using the average viscosity of CO_2 at temperatures between 800 and 950°C., the flow rate of CO_2 to produce aggregative fluidization conditions for the activation experiments was determined from Figure 1. A flow rate of 0.037 ft.³/min. (S.T.P.) was selected.

Activation experiment—Anthracite samples were devolatilized in a N_2 stream at fluidizing conditions before reacting them with CO_2. The preheater and reactor were brought to 950°C. After purging the air inside the system with N_2, the samples were fed through the pressure probe. Nitrogen was introduced at a rate of 0.04 ft.³/min. A thermocouple was inserted into the center of the fluidizing bed. The devolatilization was continued for 5 hours at 950°C. No attempt was made to analyze the product gases during devolatilization. After cooling to 100°C., the sample collector was attached to the pressure probe; and the sample was withdrawn through the probe using a vacuum pump. A small amount of alundum grains collected with the sample was separated by sieving. The devolatilized anthracite was found to contain a negligible amount of −65 mesh material, indicating no significant decrepitation of the original anthracite during devolatilization.

For the activation runs, the reactor and preheater were brought to the desired temperature. Nitrogen was introduced to purge the system. After purging for about 30 minutes, the N_2 flow was stopped and the appropriate weight of devolatilized anthracite was fed into the reactor. Nitrogen was immediately reintroduced and the sample was heated under fluidizing conditions until the center of the bed reached the desired temperature. Then, the N_2 flow was stopped and CO_2 was introduced at a preselected flow rate. After 30 minutes in CO_2, stop cock A (Figure 4)

was adjusted, so that part of the effluent gases was fed into the analysis section at a rate of approximately 0.01 ft.³/min. The remainder of the gases was led to the exhaust after passing through wet test meter No. 1. At certain time intervals the readings of the three wet test meters were taken. From these data the volume of the product gases, the CO concentration, and then the amount of carbon burn-off as a function of time could be calculated. The amount of carbon burn-off during the initial unsteady state period was estimated by extrapolation of the cumulative burn-off versus time plot to zero time. It was then possible to calculate the activation time required to reach a desired percentage of burn-off. At this predicted time, the CO_2 flow was stopped and the sample was cooled in a N_2 stream. The product sample was removed from the reactor, weighed, and the actual percentage of burn-off calculated.

Dynamic adsorption experiment—The activated sample was dried at 130°C. for 3 hours and placed in the adsorber. The flow rate of N_2 was 360 cc./min. (S.T.P.) with the flow rate in the lines *A* and *B* (see Figure 5) adjusted so that the concentration of the organic vapor (CCl_4 was used in this study) at adsorption temperature corresponded to $p/p_s = 0.21$, where p is the partial pressure of the organic vapor and p_s is the saturation pressure of the organic vapor at 25°C. At the beginning of a run, the feed gas bypassed the adsorber and went directly to the thermal conductivity cell analyzer, where the constancy of the organic vapor concentration was checked over a period of 30 minutes. Following this check, the feed gas was passed through the adsorber and the effluent gas was passed from the adsorber through a wet test meter. The thermal conductivity cell analyzer registered the concentration of the organic vapor in the effluent gas. The break point, where the organic vapor first appeared in the effluent gas, could be easily detected on the recorder chart. A run was completed when the concentration of organic vapor in the effluent stream equalled its concentration in the entering stream—that is, adsorption was complete. The amount of vapor adsorbed was determined from the weight increase of the adsorber, and the adsorptive capacity at the preselected relative pressure of adsorbate was calculated.

TABLE IV
Specific Reaction Rate of St. Nicholas Anthracite with Carbon Dioxide as a Function of Temperature and Burn-off

(First Series of Experiments)

Reaction temperature °C	Burn-off %	Average CO_2 partial pressure atm.	Specific rate constant	
			Zero-order g./g. hr.	First-order g./g. hr. atm.
800	5	0.990	0.0025	0.0025
	11	0.990	0.0031	0.0031
	22	0.990	0.0029	0.0029
	33	0.990	0.0079	0.0080
850	5	0.952	0.0076	0.0080
	11	0.965	0.0089	0.0092
	22	0.950	0.0103	0.0113
	33	0.970	0.0123	0.0125
900	5	0.928	0.0138	0.0149
	11	0.910	0.0183	0.0201
	22	0.910	0.0203	0.0223
	33	0.930	0.0253	0.0272
950	5	0.831	0.0265	0.0319
	11	0.827	0.0339	0.0410
	22	0.825	0.0476	0.0575
	33	0.860	0.0558	0.0642

(Second Series of Experiments)

850	5	0.970	0.0067	0.0070
	11	0.950	0.0086	0.0091
	22	0.950	0.0097	0.0102
	33	0.952	0.0120	0.0126
	44	0.975	0.0113	0.0116
	57	0.967	0.0166	0.0172
	65	0.965	0.0179	0.0186
950	5	0.834	0.0293	0.0352
	11	0.825	0.0392	0.0475
	22	0.813	0.0448	0.0552
	33	0.815	0.0566	0.0695
	44	0.825	0.0611	0.0741
	57	0.885	0.0827	0.0925
	65	0.885	0.0990	0.112

EXPERIMENTAL RESULTS

RATE OF REACTION OF ANTHRACITE WITH CARBON DIOXIDE

For all activation runs, an approximate linear

TABLE V
Comparison of the Pore Structure and Dynamic Adsorption Characteristics for CCl_4 between Selected Activated Anthracites and Commercial Activated Carbons

	SCR-850-38*	SCR-850-65**	PC1	PC2
Mineral matter content, %	12.1	19.9	6.8	5.3
Surface area, $m.^2/g.$	1072	1890	1610	1360
Density, g./cc.***				
Apparent	1.13_4	0.887	0.673	0.755
Helium	2.11_7	2.14_6	2.28_6	2.25_3
Total open pore volume, cc./g.	0.409	0.661	1.048	0.881
Pore volume, %				
First distribution	92	89	52	57
Second distribution	6	9	23	13
Third distribution	2	2	25	30
Pore volume, cc./g.				
First distribution	0.376	0.588	0.544	0.508
Second distribution	0.025	0.060	0.241	0.116
Third distribution	0.008	0.013	0.262	0.267
First pore volume distribution function				
μ	2.28	2.78	3.30	3.10
σ	0.73	0.57	0.57	1.15
y (maximum)	3.32	3.45	3.30	3.30
Average pore diameter of the first distribution, $\AA$	8.7	12.5	16.4	9.7
CCl_4-adsorptive capacity for p/p_s of 0.21 at 25°C., g.CCl_4/g.	0.462	0.873	0.751	0.648
Percentage of total pore volume filled with CCl_4	71.0	82.9	44.9	46.1
Break-point concentration, g. CCl_4/g.	0.404	0.813	0.705	0.602
Relative break-point concentration	0.87	0.93	0.94	0.93

* Anthracite sample activated at 850°C. to 38% burn-off.
** Anthracite sample activated at 850°C. to 65% burn-off.
*** Densities on a m.m.f.b. were calculated assuming that the density of mineral matter is 2.7 g./cc. for all samples (19).

relation was obtained between cumulative carbon burn-off and reaction time. The instantaneous, specific reaction rates calculated at various burn-offs are listed in Table IV. The specific reaction rate increased with burn-off. This increase is thought to be due to a combination of better solid-gas contact with decreasing weight of fluidized bed (7) and to greater particle utilization for reaction. This latter point implies that the rate of reaction of the anthracite with CO_2 is controlled, in part, by the rate at which the CO_2 can diffuse through the interior of the anthracite particle. For a complete discussion of this subject the reader should refer to Reference (13).

Using the rate data, Arrhenius plots were made and activation energies were calculated for various stages of burn-off. Since only two temperatures were used for the second series of experiments, activation energies were not calculated for these runs. The activation energy increased from 46 to 53 kcal./mole with increase in burn-off from 5 to 33% using the zero order specific rate constants and from 43 to 46 kcal./mole using the first order specific rate constants.

PORE STRUCTURE OF ACTIVATED ANTHRACITES

Nitrogen adsorption isotherms at 78°K.,

helium densities at 29°C., apparent densities, and macropore volume distributions (using the mercury porosimeter) were determined on most of the activated samples. From these data, surface areas, total pore volumes, pore volume distributions, and average micropore diameters (in pores less than 30A.) could be calculated. The development of the pore structure in activated anthracite as a function of reaction temperature and carbon burn-off will be published in detail later. In this paper properties of some selected samples are compared with those of the two commercial activated carbons which were examined. The properties are summarized in Table V. The pore volume distributions could be expressed by using a normal distribution function having three different sets of parameters for each sample, as follows:

$$dv = \frac{1}{\sqrt{2\pi}\sigma} \exp\left[-\frac{(y-\mu)^2}{2\sigma^2}\right] dy \qquad (1)$$

where

v pore volume in percentage,
$y = \ln D$ where D is the pore diameter in $A.$,
σ and μ are parameters.

In the order of increasing pore diameter, these three distribution functions are called the first, second and third distributions. The first distribution, in which the majority of the adsorption capacity of an activated carbon lies, had maximum pore diameters of ca. 30 A. for all four samples in Table V.

TABLE VI
Adsorptive Capacities of Activated Anthracites for CCl_4 (g.CCl_4/g.,m.m.f.b.)

Burn-off %	Activation Temperature, °C.			
	800	850	900	950
8	0.033	0.045	0.049	0.054
16	0.123	0.143	0.148	0.148
27	0.292	0.285	0.282	0.271
38	0.427	0.462	0.429	0.387
52	—	0.685	—	0.548
65	—	0.873	—	0.756

The development of surface area (the areas calculated from Langmuir plots of isotherm data) in activated anthracite as a function of burn-off at 850 and 950°C. is summarized in Figure 6. Linear relationships were obtained for samples activated at both temperatures, with a burn-off at 850°C. being somewhat more effective at opening up area.

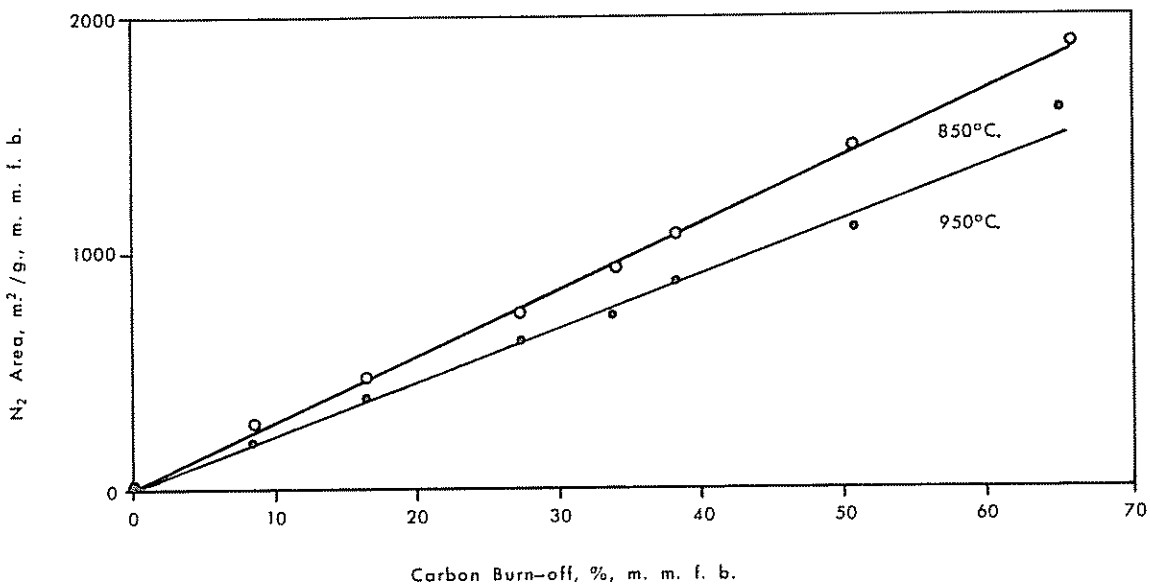

VARIATION OF NITROGEN SURFACE AREA OF ACTIVATED ANTHRACITE WITH BURN-OFF AT 850 AND 950°C.

Figure 6

DYNAMIC ADSORPTION CHARACTERISTICS

The adsorptive capacities of the activated anthracites for CCl_4 in the first series of experiments are listed in Table VI. Assuming that the mineral matter does not participate in the adsorption, these adsorptive capacities are calculated on a mineral matter-free basis. From these experimental results, it was concluded that activation temperatures between 800 and 900°C. did not have a significant effect on adsorptive capacity. The equation

$$C = 1.35(x - 0.1) + 0.06 \qquad (2)$$

describes the relationship between adsorptive capacity (C) for CCl_4 and fraction of burn-off (x) over the above temperature range up to 38% burn-off. Extrapolating this relationship to higher burn-offs, the optimum percentage of burn-off was estimated as 53% upon solving the equation $d[(C)(1 - x)]/dx = 0$. The adsorptive capacity expected at this burn-off is 0.64 g. CCl_4/g. carbon. Data for burn-offs higher than 38% are available for carbons activated at 850 and 950°C. in the second series of experiments. These results are plotted in Figure 7. Linear relationships were again found, namely

$$C = 1.49(x - 0.1) + 0.05 \qquad (3)$$

and

$$C = 1.25(x - 0.1) + 0.05 \qquad (4)$$

for activation at 850 and 950°C., respectively. A slight change in the coefficients is observed between equations (2) and (3) for activation at 850°C. in the two separate series of runs. Using equation (3), the optimum percentage of burn-off is calculated to be 53.4%, with an accompanying capacity of 0.70 g. CCl_4/g. carbon. This is in good agreement with the values predicted from the first series of experiments. The optimum conditions calculated for activation at 950°C. were 53.0% burn-off and 0.58 g. CCl_4/g. carbon.

The efficiency of dynamic adsorption may be defined by the following equation:

$$\alpha = (c_i - c_0)/c_i \qquad (5)$$

where c_i and c_0 are the concentrations of organic vapor in the carrier gas at the inlet and outlet of the adsorber. By graphical integration of the effluent gas concentration versus time plot, the amount of CCl_4 adsorbed in the bed, that is, the adsorption bed concentration, was determined. The change of adsorption efficiency with the bed concentration is shown in Figure 8 for samples activated at 850°C. at various degrees of burn-

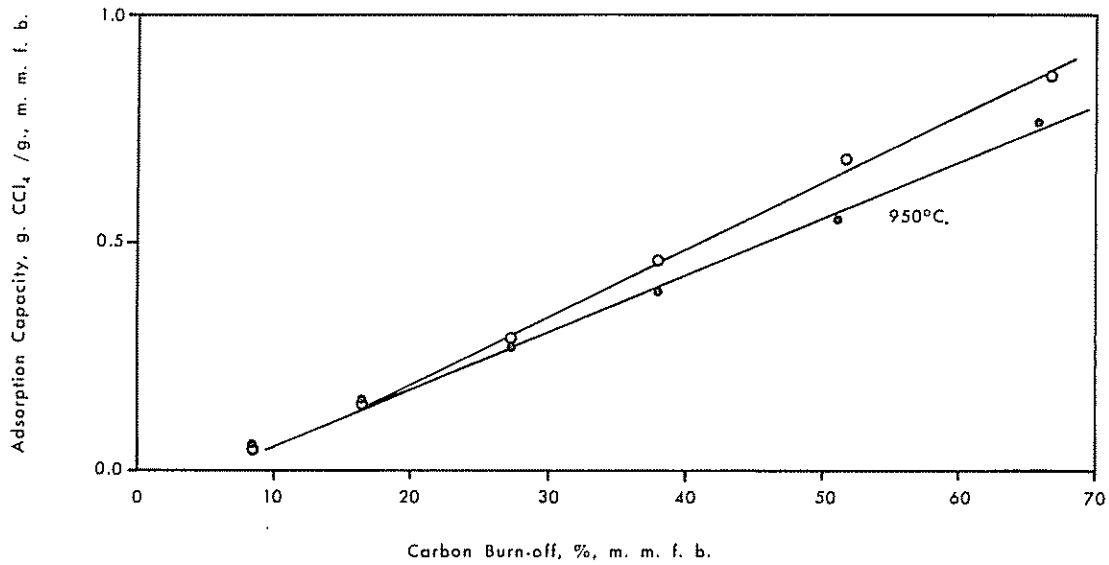

VARIATION OF ADSORPTIVE CAPACITY FOR CCl_4 OF ACTIVATED ANTHRACITE WITH BURN-OFF AT 850 AND 950°C.

Figure 7

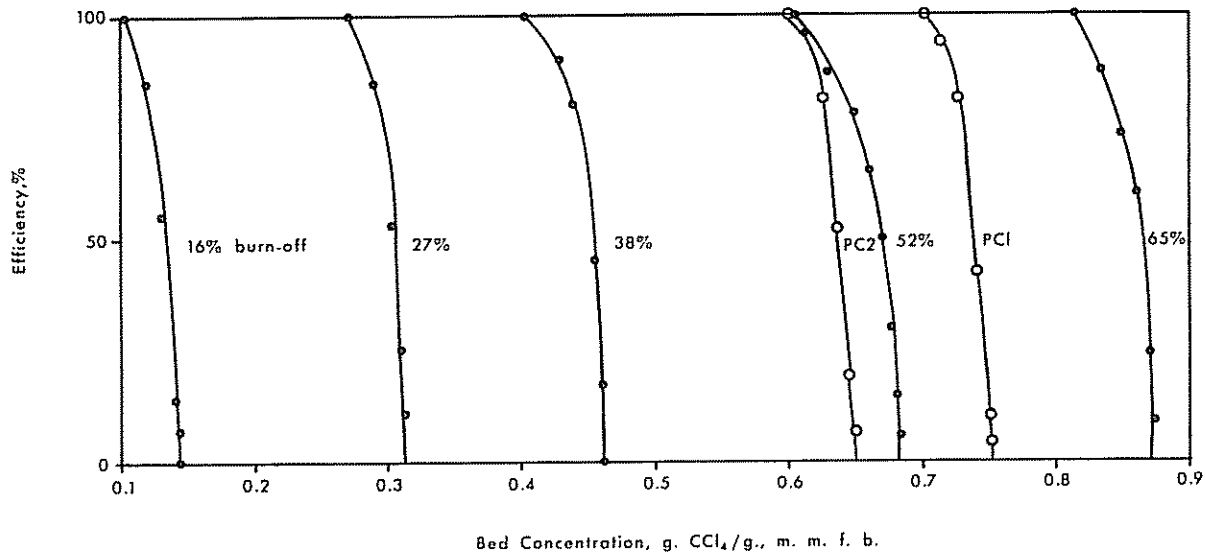

EFFICIENCY OF ADSORPTION OF CCl_4 WITH VARYING BED CONCENTRATION FOR ANTHRACITE ACTIVATED AT 850°C. AND THE COMMERCIAL CARBONS

Figure 8

offs. In Figure 8, the break-point bed concentration corresponds to the point where the efficiency first falls below 100%. The break-point concentrations are summarized in Table VII. No attempt was made to determine the break-points for the samples activated to 8% burn-off, because the break-point occurred almost instantaneously after introduction of the CCl_4 stream. The relative break-point concentrations, defined as the ratio of the break-point concentrations to the saturation concentrations, are also listed in Table VII. The relative break-point concentration varied from 0.73 to 0.93 as burn-off was increased from 16 to 65%. The dynamic adsorption characteristics of the two commercial carbons were also investigated and the results are summarized in Figure 8 and Table V.

DISCUSSION

Activated carbon used for vapor phase adsorption contains a large internal surface area of micropores having molecular dimensions. According to Dubinin (12), the strong field of the Van der Waals adsorption potential in these fine pores, which results from superposition of the field of opposite walls, is responsible for physical adsorption of vapors on activated carbons. The strongest potential field is expected to exist in the smallest pores. It is generally accepted that anthracite contains a large amount of fine pores. It was suggested by Hirsh (1) that anthracite consists of graphitic lamellae of various diameters, and the poor packing of these irregularly shaped lamellae produces pores. It is reasonable to assume that these fine pores in anthracite will provide a strong potential field for adsorption, if they are accessible to adsorption vapors. However, the total open pore volume in the raw St. Nicholas anthracite was only 0.093 cc./g. This low value for open pore volume suggests that if fine pores did exist in the raw anthracite, a majority of them were inaccessible to helium at room temperature. The production of activated carbons from anthracite may be considered then to consist of the opening up of these closed pores and the enlargement of pore sizes to an extent such that adsorbates may be able to diffuse in without losing essentially any of their adsorption potential.

In order to achieve the development of porosity most efficiently, it is desirable that the oxidizing reaction used to activate the anthracite takes place uniformly in the interior of the particle and that no external particle volume is lost. The reaction of carbon with CO_2 (used as the oxidizing gas in these studies) was described in detail by Walker, Rusinko and Austin (13).

TABLE VII

Break Point Concentrations and Relative Break-Point Concentrations for Dynamic Adsorption of CCl_4 on Activated Anthracites

Burn-off	Activation temperature, °C.							
	800		850		900		950	
%	C_b*	C_{rb}	C_b	C_{rb}	C_b	C_{rb}	C_b	C_{rb}
16	0.096	0.78	0.104	0.73	0.117	0.79	0.110	0.75
27	0.247	0.85	0.246	0.84	0.232	0.82	0.218	0.81
38	0.381	0.89	0.404	0.87	0.380	0.88	0.328	0.85
52	——	——	0.608	0.89	——	——	0.508	0.93
65	——	——	0.813	0.93	——	——	0.562	0.93

* C_b, g.CCl_4/g., m.m.f.b.

As the temperature is increased, the rate determining step or steps progressively change from the chemical rate to a combination of the chemical rate and the rate of diffusion into the internal structure, and finally to the rate of diffusion through the stagnant film surrounding the particle. The temperature ranges over which these steps control the oxidation or gasification rate are called Zones I, II, and III, respectively. In Zone I, the reaction takes place uniformly through the interior of the particle, resulting in the most efficient development of porosity. According to Walker et al., the activation energy for the reaction $C + CO_2 \rightarrow 2CO$ is about 90 kcal./mole in Zone I, half of this value in Zone II, and less than 5 kcal./mole in Zone III. In this investigation, the over-all activation energy varied from 46 to 53 kcal./mole as the carbon burn-off proceeded from 5 to 33%. It indicates that over the temperature range investigated, the reaction rate is controlled jointly by the chemical rate and the rate of diffusion of CO_2 into the internal pore structure. The increase in activation energy with burn-off implies that the development of internal pore structure tends to increase the rate of internal diffusion of CO_2 and consequently to decrease the contribution of the internal diffusion resistance in determining the reaction rate.

The adsorptive capacity of the activated anthracites for CCl_4 increased linearly with burn-off as shown in Figure 8. This increase is paralleled by a similar, linear increase in surface area with increasing burn-off, as shown in Figure 6. The optimum percentage of burn-off on the basis of surface area (that is, the percentage of burn-off where the maximum total area is obtained) is calculated to be about 50% for activation temperatures of 850 and 950°C. The optimum percentage of burn-off on the basis of CCl_4-adsorption capacity is calculated to be about 53%. Therefore, good agreement between these two optimum conditions is observed.

When activated carbons are used for vapor phase adsorption processes in the chemical industry, the break-point concentration is often more important than total adsorptive capacity. The break-point concentration is governed by the rate of mass transfer in the adsorption bed in addition to the adsorptive capacity. The mass transfer coefficient of the adsorption process can be expressed by the following equation:

$$K\Delta P = \frac{\Delta p_f + \Delta p_d + \Delta p_a}{\frac{1}{k_f} + \frac{1}{k_d} + \frac{1}{k_a}} \qquad (6)$$

where K and k are the mass transfer coefficients, over-all and individual, respectively; ΔP and Δp are the over-all and individual pressure gradients; and the subscripts f, d, and a symbolize mass transfer through the stagnant film, mass transfer into the internal pore structure by diffusion, and adsorption of CCl_4 on the carbon surface, respectively. According to Hsu and Molstad (14), the over-all mass transfer coefficient for CCl_4 in a fluidized bed of activated carbons is controlled by k_f up to relative bed concentrations of about 0.7. Beyond this point, the over-all mass transfer

coefficient falls off rapidly, indicating that the mass transfer rate is controlled by k_d. Usually the value of k_a is much greater than either k_f or k_d for this type of process (14). As the bed concentration increases, narrowing of pores and possible blocking of pore mouths by adsorbate appear to hinder diffusion of the adsorbate through the pore, causing the falling-off of the over-all mass transfer rate. The complete analysis of the break-point phenomenon involves numerous factors, such as, the flow rate of the gas, particle size, bed weight, and the nature of the pore structure of the adsorbent. Details of the analysis of the break-point phenomenon are being studied in this laboratory. In this investigation, arbitrary conditions were set so that the break-point concentration and the mode of efficiency fall-off with increase in bed concentration were observed for various samples. Several testing methods have appeared in the literature. Except for the flow rate of the carrier gas, most previous experimental conditions used were similar to those employed in this investigation. The linear flow rates previously employed varied from 2.7 to 16.7 cm./sec. The relative pressure of CCl_4 most frequently used was 0.30. In this investigation, the flow rate was 9.8 cm./sec. and the concentration of CCl_4 corresponded to a relative pressure of 0.21 at adsorption conditions. In this work, the break-point concentrations increased with burn-off, paralleling the increase of adsorptive capacity. For all samples, there was no significant change in the mode of efficiency fall-off beyond the break point. The relative break point concentration, however, increased from 0.73 to 0.93 for the samples activated at 850°C., as burn-off was increased from 16 to 65%. A similar increase in break-point concentration with increasing burn-off was also found for samples activated at other temperatures.

Upon further analysis of equation (6), the diffusion mass transfer coefficient k_d can be divided into three terms, depending on different diffusion mechanisms. Usually the pore volume distribution of activated carbons can be separated into micro, transitional, and macropores (15, 16). The diffusion mechanism in macropores will be that given by normal bulk diffusion concepts, whereas the diffusion mechanism in transitional and micropores will be given usually by Knudsen diffusion concepts. In addition to these two diffusion mechanisms, surface diffusion of adsorbate molecules, that is two dimensional movement of molecules on pore walls, can take place in the micropores (17). Applying the Dubinin hypothesis of branching among the three types of pores (16), it can be considered that the rate of the first two diffusion steps governs the rate of mass transfer from the exterior of the particle to the micropores at the interior, where adsorption takes place. The rate of surface diffusion can control the accessibility of micropores to incoming adsorbate molecules. Thus, when considering the rate of dynamic adsorption, the pore volume, pore size, pore volume distribution, and the extent of interconnection of pores will be of importance, since these factors control the rate of diffusion.

The first, second, and third pore size distributions shown in this paper (Table V) probably correspond to the collection of micro, transitional, and macropores mentioned above. The first, second, and third distributions cover, respectively, pores of diameter less than 30 A., from 30 to about 10,000 A., and higher than 10,000 A. As shown in Table V, the two commercial carbons have much larger pore volumes in the second and third distributions than do the activated anthracites. However, despite this large difference in pore volume distribution between activated anthracites and commercial carbons, there was no major difference in the mode of efficiency fall-off beyond the break-point, as shown in Figure 8. Also the difference in the relative break-point concentrations was small as shown in Table V. These facts suggest that the diffusion of adsorbate from the exterior to the internal micropores is not rate controlling under the experimental conditions employed. Thus, it is suggested that the diffusion of the adsorbate through the stagnant film is the rate determining step at low bed concentrations, followed by surface and/or Knudsen diffusion in the micropores which become the rate determining step at high bed concentrations. Also the increase of the relative break-point concentration with burn-off could be attributed to a better interconnection of pores, which is a result of increase in pore volume as burn-off proceeds.

In comparing the pore structure between activated anthracites and bituminous coal-based activated carbons, as shown in Table V, the most significant difference is the pore volume distributions, as mentioned above. The manufacturing process of commercial activated carbons includes briquetting of coal with a binder prior to activation. It is probable that the activated binder

is responsible for the considerable volume of large pores which these samples possess. As shown in Table V, the anthracite activated at 850°C. to 65% burn-off is superior to the commercial carbons if extent of surface area, micropore volume, and/or CCl_4-adsorptive capacity are used as criteria.

In this investigation the effect of temperature and burn-off on the development of pore structure was thoroughly investigated for a particular particle size of anthracite and the optimum conditions for a manufacturing process of activated carbons was determined. The optimum conditions were found to be ca. 50% burn-off at temperatures between 800 and 900°C. Activated anthracites produced at this condition were found to have 0.47 cc./g. of pore volume, 1400 $m.^2/g.$ of surface area, and 0.70 g. $CCl_4/g.$ of adsorptive capacity. These values compare favorably with those of commercial carbons. However, one possible drawback to the activated anthracite is its high mineral matter content. It is thought that steam is superior to CO_2 as an activating agent; that is, it produces a higher adsorptive capacity for less burn-off.‡ Thus, steam activation would result in an activated carbon having a lower mineral matter content. Also the removal of mineral matter from anthracite by high temperature chlorination has been shown to be feasible in this laboratory (18), and a combination of this process with steam activation of anthracite may be a good solution for decreasing mineral matter content. Considering the market price of anthracite, the abundant reserves of anthracite in Pennsylvania, and the fairly simple process for activation, the manufacture of activated carbons from anthracite appears to be promising.

Work is continuing to clarify: the effect of activating agent, raw anthracite, and particle size of anthracite on the properties of the material produced. Also, studies on dynamic and static adsorption characteristics of the product carbons for various organic vapors are being continued.

ACKNOWLEDGMENT

The authors wish to acknowledge the generous support of The Commonwealth of Pennsylvania and the Pennsylvania Anthracite Industry for the financial support which made this work possible. Special thanks are extended to the Pittsburgh Chemical Company for supplying the commercial activated carbons.

‡ Carbon dioxide was selected as the activating gas in this research rather than steam since the $C—CO_2$ reaction lends itself to interpretation more easily than does the $C—H_2O$ reaction with its many subsequent side reactions.

REFERENCES

1. Hirsch, P. B., Proc. Roy. Soc. (London), *A226*, 143 (1954).
2. Bond, R. L. and Spencer, D. H. T., Ind. Carbon and Graphite Conf., London, pp. 231–251 (1958).
3. Anderson, R. B., Hall, W. K., Lecky, J. A., and Stein, K. C., J. Phys. Chem., *60*, 1548 (1956).
4. Clendenin, J. D., Griffiths, W. T., and Wright, C. C., Trans. Annual Anthracite Conf., Lehigh Univ., *10*, 121 (1952).
5. Hassler, J. W., Proc. Anthracite Conf., Bull. Mineral Inds. Expt. Sta., Pennsylvania State Univ., No. 70, pp. 1–5 (1957).
6. Hassler, J. W., Chem. Eng. Progr., *52*, No. 12,56 (1956).
7. Williams, D. A., Ph.D. thesis, The University of Sheffield (1953).
8. Leva, M., Grummer, M., Weintraub, M., and Pollchik, M., Chem. Eng. Progr., *44*, 511 (1948).
9. Leva, M., Weintraub, M., and Pollchik, M., Ind. Eng. Chem., *41*, 1206 (1949).
10. Walker, P. L., Jr., Foresti, R. J., Jr., and Wright, C. C., Ind. Eng. Chem., *45*, 1703 (1953).
11. Raats, E., Ph.D. thesis, The Pennsylvania State University (1955).
12. Geller, I., Ph.D. thesis, The Pennsylvania State University (1959).
13. Walker, P. L., Jr., Rusinko, F., Jr., and Austin, L. G., "Gas Reactions of Carbon," in *Advances in Catalysis*, Vol. XI, pp. 133–221, Academic Press Inc., New York, N. Y., (1959).
14. Hsu, C. T., and Molstad, M. C., Ind. Eng. Chem., *47*, 1550 (1955).
15. Dubinin, M., Ind. Carbon and Graphite, London, pp. 219–230 (1958).

16. Dubinin, M. M., Zhuk, G. S., and Zaverina, E. D., Zhur. Fiz. Khim., *31*, 1126 (1957).

17. Carman, P. C., "Flow of Gases through Porous Media," p. 105, Academic Press Inc., New York, N. Y. (1956).

18. Imperial, G., and Walker, P. L. Jr., "Removal of Mineral Matter from Anthracite by Chlorination at High Temperatures," Report to the Coal Research Board of the Commonwealth of Pennsylvania, The Pennsylvania State Univ., No. SR-12 (1959).

19. Wandless, A. M., and Macrae, J. C., Fuel (London), *13*, 4 (1934).

DEFINITION OF SYMBOLS FOR PRELIMINARY STUDY ON FLUIDIZATION

D_p Particle diameter, ft.

G Mass velocity of the fluid, lb./(ft.)^2(hr.)

l Height of bed, ft.

l Height of bed, ft.

l_{mf} Minimum fluidization bed height, ft.

m The slope of the plot ln (GR/γ_f) vs. ln $[\epsilon^3/(1-\epsilon)^2]$

Δp Pressure drop, lb./ft.^{2}

R l/l_{mf}, dimensionless bed expansion ratio

u Linear velocity of fluid, ft./sec.

u_{ma} Critical (minimum) aggregative fluidization velocity, ft./sec.

u_{mf} Critical (minimum) quiescent fluidization velocity, ft./sec.

u_{ms} Critical (minimum) slugging velocity, ft./sec.

γ_a Apparent density of particle, lb./ft.^{3}

γ_{bc} Critical bulk density of bed, (minimum fluidization bed density), lb./ft.^{3}

γ_f Density of fluid, lb/ft.^{3}

ϵ Fraction bed voidage, dimensionless

μ Viscosity of fluid, (lb.)/(ft.)(hr.)